Natural Fragment Bond Orbital Method for Inter-Fragment Bonding Interaction Analysis

Yichi Zhang,* Fu Kit Sheong, and Zhenyang Lin*

Department of Chemistry, The Hong Kong University of Science and Technology, Kowloon, Hong Kong, China

E-mail: yzhangnn@connect.ust.hk; chzlin@ust.hk

Abstract

A complex chemical system is often examined based on their fragments, so fragment-based analysis is the key to chemical understanding. We report the natural fragment bond orbital (NFBO) method for inter-fragment bonding interaction analysis, as an extension to the well-known natural bond orbital method. NFBOs together with their corresponding natural fragment hybrid orbitals (NFHOs) allow us to derive local bonding and anti-bonding orbitals among fragments from the delocalized canonical molecular orbitals. In this paper, we provide the algorithm for finding NFBOs and showcase its application to several chemically interesting systems featuring significant inter-fragment bonding interactions. Through these examples, the NFBO method is shown to be a powerful tool for molecules possessing strong inter-fragment bonding interactions.

1 Introduction

Chemists commonly perceive material world as a collection of molecules, and molecules as a collection of chemically meaningful molecular fragments. Many molecular properties, including stability and reactivity, are closely intertwined with the bonding interactions occurring

among the constituent molecular fragments. Consequently, understanding the bonding interactions among these material or molecular fragments becomes a fundamental aspect of chemistry.

However, current molecular orbital calculations, which provide valuable insights into bonding interactions, often yield results that exhibit significant delocalization over the entire molecular system, making it challenging to observe inter-fragment interactions. Conversely, available localization techniques view molecular orbitals as combinations of localized orbitals centered on minimal regions, dividing fragments into smaller units akin to atoms.[1–4] In both cases, a fragment representation of the wavefunctions (orbitals) consistent with the intuition remains elusive. Consequently, the development of orbital analysis methods specifically tailored for inter-fragment bonding interactions is imperative.

A successful attempt to clearly demonstrate two-fragment orbital interactions is the principal interacting orbital (PIO) analysis.[5–7] The PIO analysis is designed to find as few orbitals as possible that are able to describe the inter-fragment bonding interactions concisely. However, in the cases with more than two fragments, one has to put the fragments into two groups and treat each group as a fragment.[7–10] Clearly, the PIO analysis has limitations when applied to scenarios where the consideration of bonding interactions involving three or more fragments becomes more meaningful.

The algorithm used by the natural bond orbital (NBO) method inspired us with a possible realization of carrying out bonding interaction analysis among more than two fragments.[11–15] As a mature technique dating back to the 1980s, NBO analysis has facilitated numerous studies on electronic structure and is still most widely used today. The application scope of NBO covers analyzing metal-to-ligand back bonding,[16,17] deciphering delocalized bonds,[18] explaining the famous 18-electron rule[19] and demystifying stereoelectronic effect of bis-peroxides,[20] etc. In addition, NBO lays the foundation for more bonding analysis tools to be built upon, such as natural localized molecular orbitals,[21] (quadratic programming) natural resonance theory,[22,23] adaptive natural density partitioning[24] and resonance natural bond orbital.[25]

We hereby put forward the natural fragment bond orbital (NFBO) method, another extension to the NBO method. While NBO is designed to reveal the bonding interactions between atoms, NFBO is designed to reveal the bonding interactions between fragments. To be specific, in the NBO method, the inter-atomic bond orbitals are searched for, while in the NFBO method, the inter-fragment bond orbitals are to be found instead. By the end of NFBO analysis, a set of natural fragment hybrid orbitals (NFHOs) is also exported, analogous to natural hybrid orbitals (NHOs) in the NBO method.[11] NFHOs are fragment orbitals that contribute to the NFBOs by linear combination.

In this paper, not only do we report the NFBO algorithm, but we also demonstrate its application to some chemically interesting systems, including the transition state of Diels-Alder reaction of a highly conjugated diene, the tri-zinc cluster $[Zn_3Cp_3]^+$,[26] the tri-thorium cluster $[\{Th(C_8H_8)Cl_2\}_3]^{2-}$,[27] the planar concentric cluster B_{19}^-[28] and the double helical semiconducting material $[Sn_7I_7P_7]_n$.[29] The common feature among these chemical systems is that they can all be naturally separated into several fragments, and the inter-fragment bonding interactions determine their stability or reactivity. Therefore, they make good examples for demonstrating the value of NFBO analysis. In the last example, we even extend this method to periodic solid state systems, where orbital interaction analysis meets difficulties.[30] We will show that their NFBO analysis results satisfy general chemical intuition.

2 Computational details

All the structures are optimized with the density functional B3LYP[31] and the basis set 6-31G(d),[32] unless otherwise noted, with the program `Gaussian 16, Revision C.01`.[33] For each example, the wavefunction obtained for the optimized structure is used for NFBO analysis. Only pure basis functions are used in the calculations, so cartesian-to-pure transformation is not needed.[34] The wavefunction file is then converted to `mwfn` format with `Multiwfn`.[35] The new wavefunction file is fed to our package `Orbaplaw`[36] for NFBO analysis.

We set the occupation threshold, a value which we will explain in Sect. 3.1, to 1.8 e per orbital, unless otherwise noted. Finally, `Multiwfn` and `VMD`[37] are used together to generate the orbital plots, with an isovalue of 0.05 au.

3 Algorithm

The algorithm for NFBOs and NFHOs are analogous to that for NBOs and NHOs, except that in this work fragments take the role of atoms.[11] For the sake of easy reproduction by interested researchers, we provide the detailed algorithm here. A graphical demonstration of the procedure (Figs. 1 and 2) is also presented to make the algorithm easier to understand. The demonstration is based on cyclic C_3HFCl^+, which is intentionally optimized with the minimal basis set STO-6G[38] instead of 6-31G(d)[32] to maintain a small matrix for illustration purpose.

3.1 Searching for inter-fragment bonding orbitals

In the first stage, we search the density matrix for electron pairs, ranging from localized ones centered at individual fragments to delocalized ones spanning across multiple fragments. The resulting orbitals that accomodate the electron pairs are called primitive NFBOs (pNFBOs). Theses pNFBOs capture the main feature of the intra-fragment and inter-fragment bonding.

1. *Grouping atoms into fragments.* The fragmentation depends on the bonding interactions to be investigated. For example, C_3HFCl^+ can be considered as a combination of three fragments, $[C^1{-}H]$, $[C^2{-}F]$ and $[C^3{-}Cl]$, where the superscripts are the indices of the carbon atoms.

2. *Obtaining the NAO-based density matrix.* The natural atomic orbitals (NAOs) make a well-behaved basis set, since they reflect the shell structure of atoms in the molecular environment and are mutually orthogonal.[34] In this step, we transform the density matrix into the NAO basis set.

3. *Identification of bonding and/or non-bonding orbitals within individual fragments.* Each block of the density matrix, whose rows and columns are related to the NAOs belonging to each fragment, is diagonalized (Fig. 1a left). The density associated with eigenvectors having eigenvalues close to full occupation within a pre-specified threshold (typically set to 1.8 e by default, as mentioned in the last section) is excluded from the total density matrix, while the remaining eigenvectors are retained (Fig. 1a left). The excluded eigenvectors correspond to bonding and/or non-bonding orbitals within individual fragments (Fig. 1a right). In the case of the cyclic C_3HFCl^+ molecule, there are eighteen excluded eigenvectors. These eigenvectors are one-fragment pNFBOs and correspond to (1) C^1−H, C^2−F and C^3−Cl σ bonds (three in total), (2) lone pairs of electrons on fluoride and chloride (six in total) and (3) core electron pairs of C, F and Cl (nine in total) (Fig. 1a bottom).

4. *Identification of two-fragment bonding orbitals.* The remaining density matrix no longer contains bonding and/or non-bonding density within individual fragments (Fig. 1b,c left). To find the two-fragment bonding orbitals, one diagonalizes the larger block corresponding to each pair of fragments (Fig. 1b,c left). Again, the eigenvectors with eigenvalues close to full occupation are considered as two-fragment bonding orbitals (Fig. 1b,c right), and their density is then removed from the density matrix for the next step below. pNFBOs 19, 20 and 21 shown at the bottom of Fig. 1b,c describe approximately the three C−C σ bonds in the cyclic C_3HFCl^+ molecule.

5. *Identification of three-or-more-fragment bonding orbitals.* Some systems have delocalized bonds among three or more fragments. To find these bonds, one searches for three-fragment bonding orbitals, four-fragment bonding orbitals, etc., successively, in the same manner described above (Fig. 1d right). pNFBO 22 shown at the bottom of Fig. 1d describes the delocalized 3c-2e π bond in the cyclic C_3HFCl^+ molecule.

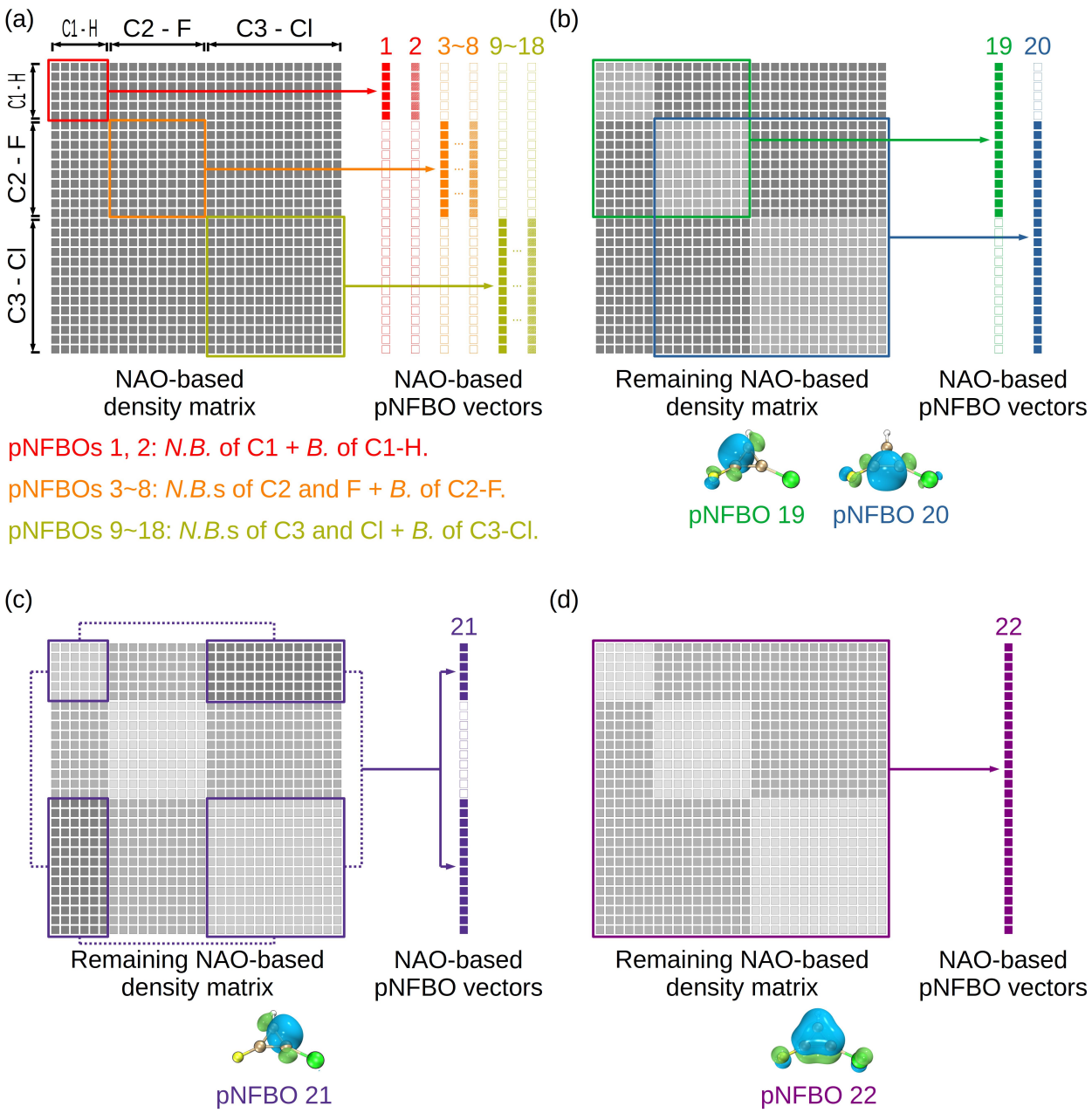

Figure 1: Schemes of identification of (a) bonding and/or non-bonding orbitals within individual fragments, (b,c) two-fragment bonding orbitals and (d) three-fragment bonding orbitals. The fragments that the rows (and columns) belong to are marked for the density matrix and the pNFBO vectors. "N.B." and "B." are short for "non-bonding orbital" and "bonding orbital", respectively. The density corresponding to previous pNFBOs are already eliminated from the paler grey regions in the remaining density matrices. The white boxes in the pNFBO vectors represent elements equal to zero by construction. The real space pNFBO plots are also shown. The colors (1) red, (2) orange, (3) yellow, (4) green, (5) blue, (6) indigo and (7) purple are linked to (1) the $[C^1{-}H]$ fragment, (2) the $[C^2{-}F]$ fragment, (3) the $[C^3{-}Cl]$ fragment, (4) the combination of the $[C^1{-}H]$ and $[C^2{-}F]$ fragments, (5) the combination of the $[C^2{-}F]$ and $[C^3{-}Cl]$ fragments, (6) the combination of the $[C^1{-}H]$ and $[C^3{-}Cl]$ fragments and (7) the combination of all the three fragments.

3.2 Generation of NFHOs and NFBOs

In the second stage, we derive the desired NFHOs and NFBOs from their primitive counterparts.

1. *(Optional) Partial localization of bonding pNFBOs onto fragments.* In degenerate pNFBOs, various linear combinations among them are possible. Therefore, the obtained pNFBOs may deviate from the generally accepted representations. In such cases, we have found that applying partial Pipek-Mezey localization[3] with Lowdin population of fragments (instead of atoms) among degenerate pNFBOs alleviates this issue to some extent.

2. *Decomposing pNFBOs into pNFHOs.* All bonding pNFBOs are decomposed according to the NAOs of the fragments involved. For example, the two-fragment pNFBO 19 is directly divided into two subvectors, one comprising the NAOs of the fragment [C^1−H] and the other of the fragment [C^2−F] (Fig. 2a). These subvectors are called primitive NFHOs (pNFHOs), embodying fragment contributions to bonding. For non-bonding orbitals (such as pNFBOs 1-18 in Fig. 2a left), a pNFBO is also a pNFHO.

3. *Orthogonalization of pNFHOs.* Fragment-wise orthogonalization of pNFHOs is carried out and results in NFHOs. As an example, pNFHOs 1, 2, 19, 23 and 25 are orthogonalized together since they belong to the same fragment [C^1−H] (Fig. 2a right). Here, an occupancy-weighted symmetric orthogonalization[34,39] is performed. The resulting NFHOs make an orthonormal basis set (Fig. 2b).

4. *Population of NFHOs.* The density matrix is projected to the NFHO basis set (Fig. 2c left). Its diagonal elements serve as occupation numbers.

5. *Generation of NFBOs.* Diagonalization of each block of the NFHO-based density matrix originating from the same pNFBO gives the final NFBOs (Fig. 2c). The eigenvalues are the occupation numbers of NFBOs, including the almost fully occupied ones with

occupation numbers to be nearly 2.0 e and the almost unoccupied ones with occupation numbers to be nearly 0.0 e. During the diagonalization, the off-diagonal blocks are expected to be approximately zero and thus ignored.

6. *(Optional) Partial localization of degenerate NFBOs upon fragments.* Again, the diagonalization in the last step may result in mixing of (nearly) degenerate orbitals. Therefore, we choose to partially localize them within their respective spaces, as mentioned in one of the previous steps.

4 Applications

In this section, we provide five examples to demonstrate the application of the NFBO method.

4.1 Diels-Alder reaction between dodecahexaene and ethene

We will begin with a simple system that involves only interactions between two fragments, yet enough to pose challenges to many existing analysis tools, the Diels-Alder reaction. In a Diels-Alder reaction, electrons flow from the HOMO of one molecule to the LUMO of the other, as well as from the HOMO of the other molecule to the LUMO of the original molecule. For small conjugated dienes, such as butadiene, the HOMO and LUMO center at the reaction site. For highly conjugated dienes, such as dodecahexaene, however, the frontier orbitals of the diene's reaction site are contaminated by other parts of the π system extending throughout the whole molecule, blurring the inter-fragment bonding interaction feature (Fig. 3). The principal interacting orbitals[5,7] and frontier molecular orbitalets[40] are two rare examples that can successfully represent the orbital interactions in this case. Here we present our NFBO analysis for this problem.

The diene and the dienophile are taken to be two fragments. As a result of NFBO analysis, inter-fragment bonding interactions involving two pairs of electrons are found. NFBOs 1 and 2 form a pair of bonding and anti-bonding orbitals, while NFBOs 3 and 4 form the other

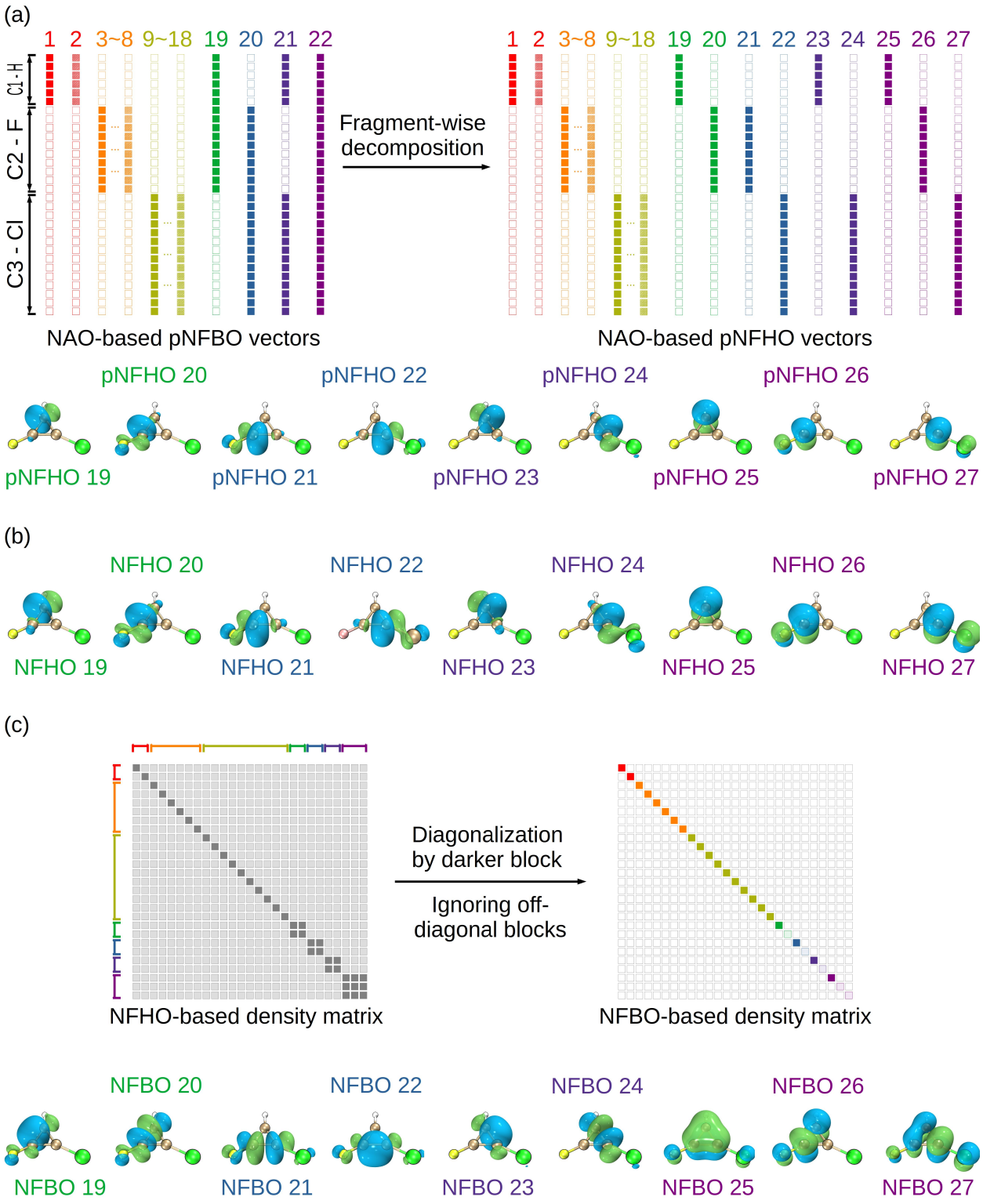

Figure 2: (a) A scheme of decomposing pNFBOs into pNFHOs; (b) A scheme of obtaining the NFHOs by fragment-wise orthogonalization; (c) A scheme of obtaining the NFBOs by diagonalization of the NFHO-based density matrix. The fragments that the NAOs belong to are marked for pNFBO and pNFHO vectors. The white boxes represent elements that are equal to zero by construction. The paler dark regions are theoretically approximately zero by construction. The paler colored regions indicate very low occupation numbers of (nearly) unoccupied NFBOs. The real space pNFHO,[9]NFHO and NFBO plots are also shown. The colors here have the same meanings as in Fig. 1.

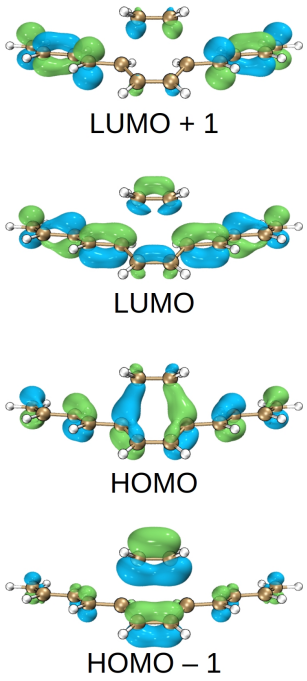

Figure 3: The frontier canonical molecular orbitals of the Diels-Alder transition state with C_s symmetry for the reaction of dodecahexaene with ethylene.

(Fig. 4). NFBOs 1 and 3 are bonding orbitals while NFBOs 2 and 4 are anti-bonding ones. They are found to be composed of the NFHOs by linear combinations, with the combination weights shown by percentages (Fig. 4). NFHOs 1 and 3 are located on the diene fragment while NFHOs 2 and 4 are on the dienophile fragment. In this way, local orbital interactions and fragment contributions to them are highlighted by NFBO analysis, against the delocalized feature of canonical molecular orbitals (Fig. 3). Besides, respective domination of the symmetric bonding orbitals by NFHOs of the dienophile and the anti-symmetric bonding orbitals by NFHOs of the diene indicates the electron flow directions in both irreducible representation spaces.

Note that the NFBOs and the NFHOs resemble the principal interacting molecular orbitals and the principal interacting orbitals in the same example given in the literature,[5,7] suggesting the same physical meaning shared by both methods.

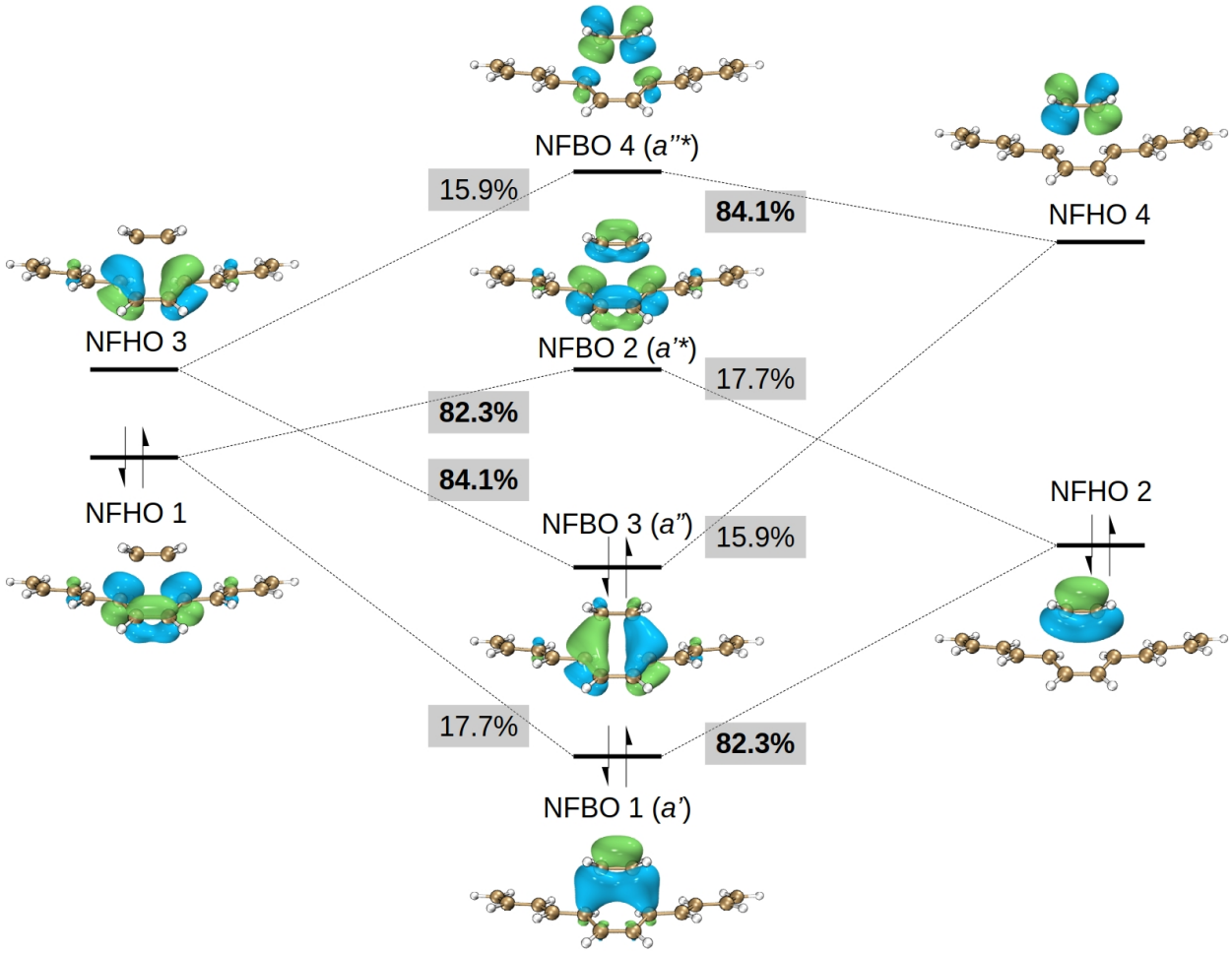

Figure 4: The NFBOs and NFHOs of the Diels-Alder transition state with C_s symmetry. The percentage on each dashed line connecting one NFBO and one NFHO is the weight, or the square of the linear combination coefficient, of this NFHO contributing to this NFBO.

4.2 The delocalized σ bonds in $[Zn_3Cp_3]^+$ and $[\{Th(C_8H_8)Cl_2\}_3]^{2-}$

The core value of the NFBO method lies on the ability to identify and quantify bonding interactions among three or more fragments. The second and third example molecules are $[Zn_3Cp_3]^+$ and $[\{Th(C_8H_8)Cl_2\}_3]^{2-}$. They both feature a delocalized σ bond among the three metal atoms, which form an equilateral triangle.

The structure of $[Zn_3Cp^*_3]^+$ was reported in Ref. 26. It was obtained by coordinating $[Cp^*{-}Zn{-}Zn{-}Cp^*]$, a linear cluster having a Zn−Zn σ bond, with the electrophilic species $[Cp^*{-}Zn]^+$. The coordination converts the σ bond to a μ_3 dangling electron pair, or a delocalized σ bond, and thus leads to formation of $[Zn_3Cp^*_3]^+$.[26,41]

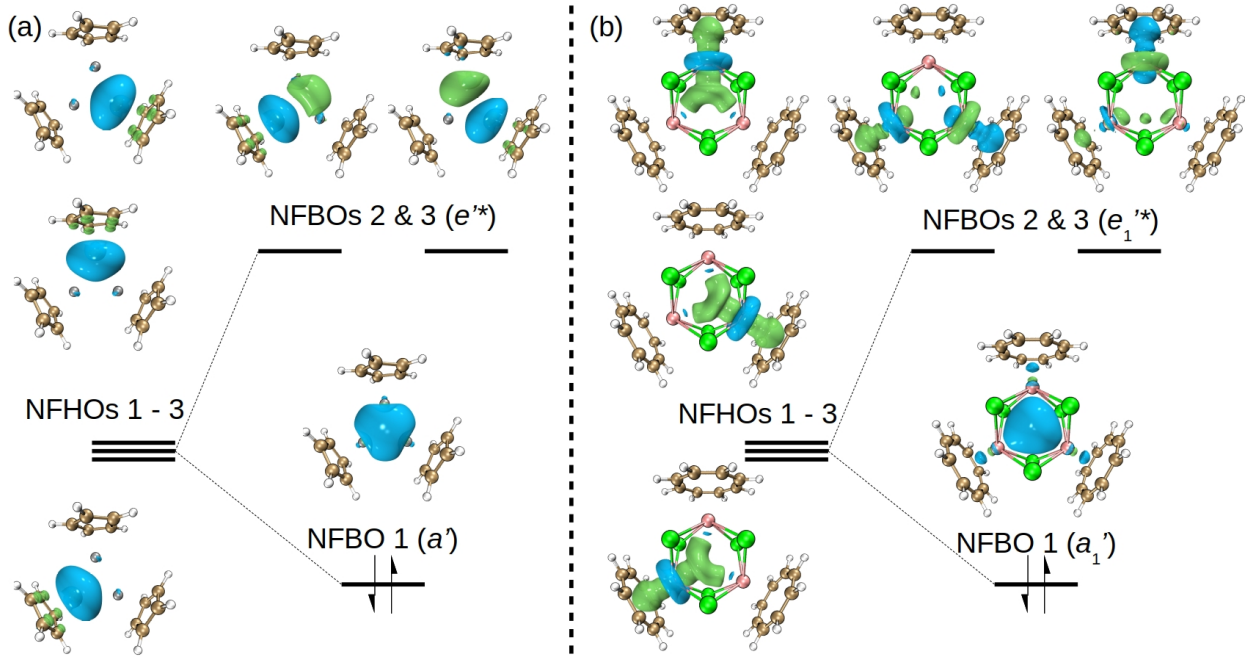

Figure 5: The NFBOs and NFHOs of the delocalized σ bond in (a) $[Zn_3Cp_3]^+$ with C_{3h} symmetry and (b) $[\{Th(C_8H_8)Cl_2\}_3]^{2-}$ with D_{3h} symmetry.

In this example, we examine its homologue, $[Zn_3Cp_3]^+$, for simplicity, with NFBO analysis. The three [Zn−Cp] units are considered as the three fragments. The analysis indicates that only a three-fragment bonding interaction is found (Fig. 5a). That means that the aforementioned delocalized σ bond is the only factor that holds the three fragments together, as expected. This delocalized σ bond is the result of interaction among the three

NFHOs centered at the three Zn atoms (Fig. 5a): An in-phase combination of these NFHOs gives the only bonding NFBO 1 with the irreducible representation a', while NFBOs 2 and 3 are anti-bonding orbitals with the irreducible representation e' (Fig. 5a).

In 2021, Boronski et al. reported $[\{Th(C_8H_8)Cl_2\}_3]^{2-}$, a crystalline tri-thorium cluster with so-called σ-aromatic metal–metal bonding (Fig. 6a).[27] Since then, there has been a hot debate on whether the aromaticity is real.[42,43] Here we analyze the metal-metal bonding interaction with our NFBO method.

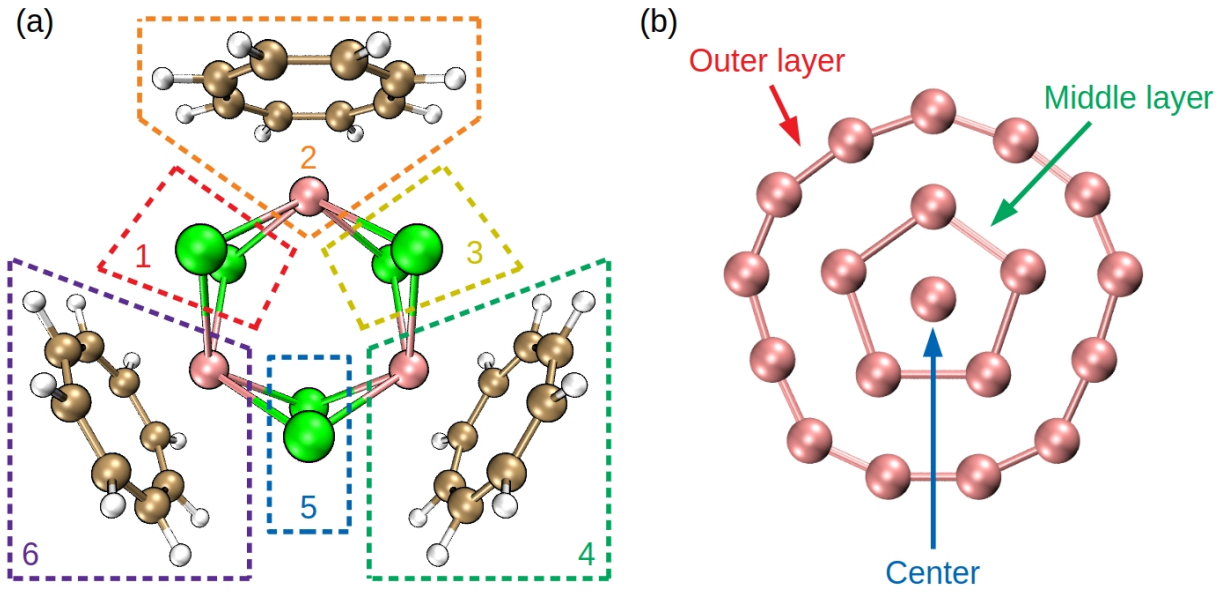

Figure 6: The geometries of (a) $[\{Th(C_8H_8)Cl_2\}_3]^{2-}$ with D_{3h} symmetry and (b) B_{19}^- with C_{2v} symmetry and their fragmentation schemes for NFBO analysis.

For this cluster, there seems no clear cut between fragments, due to the bridging Cl atoms connecting the three Th atoms. However, we still need to put the three Th atoms in three fragments since we are going to investigate their bonding interaction. Therefore, we choose to assign the three $[Th-C_8H_8]$ units to three separate fragments and the six Cl atoms pair-wisely to three fragments (Fig. 6a). Besides, we set the occupation threshold to 1.9 e per orbital in this example. In the DFT computation, we use the relativistic pseudo-potential basis set MWB60[44] for Th.

With NFBO analysis, we find no two-fragment bonds between any pair of the three

[Th−C_8H_8] units. Instead, we find a three-fragment bond at the center of the cage (Fig. 5b), with one bonding orbital (NFBO 1) and two anti-bonding orbitals (NFBOs 2 and 3). They are the linear combinations of the NFHOs that resemble the d_{z^2} orbitals of the three Th atoms in shape. Therefore, we conclude that NFBO analysis suggests a three-center delocalized σ bond at the center of $[\{Th(C_8H_8)Cl_2\}_3]^{2-}$, which involves the d_{z^2} orbitals of the Th atoms. (Here, the z axis is defined as the radial vector from the center of the metal triangle to each Th atom.)

Additionally, light is shed upon the nature of type-III mixed valence in these two examples.[45] Without locating the delocalized σ bonds among the metal centers, each Zn atom has an oxidation state of $+\frac{2}{3}$, while each Th atom has an oxidation state of $+\frac{11}{3}$. Removing the tri-metallic delocalized electrons from the total negative charge renders the metal centers to be Zn(0) and Th(III). In this way, the NFBO method has aided our understanding of the type-III mixed valences of the metal atoms in these systems. We have also resolved the mixed valence problem in a tri-titanium polyhydride complex introduced in Ref. 46 (See "Code availability").

4.3 B_{19}^-: A 2-D three-layer cluster

In 2010, Huang et al. reported an all-boron cluster B_{19}^-.[28] In 2021, Li et al. revised the previous view on the electronic structure of B_{19}^-, and proposed a scheme of inner $2\pi/6\sigma$ and outer $10\pi/14\sigma$ aromaticity, with the adaptive natural density partitioning (AdNDP) method[24] combined with canonical molecular orbital analysis, to explain the stability of this cluster.[47] In this section, we use NFBO to analyze its bonding. We will see that NFBO analysis produces a bonding picture somewhat similar to Li's work.

B_{19}^- has a 2-D concentric three-layer geometry, with one atom at the center, five atoms in the middle layer and thirteen atoms in the outer layer (Fig. 6b). Since each layer naturally forms a fragment, NFBO analysis is suitable for this cluster. Based on this fragmentation scheme (Fig. 6b), Fig. 7 lists all the important occupied NFBOs of B_{19}^-. Excluding all the

core orbitals and the thirteen B−B single bonds in the outer layer, there are three σ and one π NFBOs between the center and the middle layer (Figs. 7a,b), seven σ and four π NFBOs between the middle layer and the outer layer (Figs. 7c,e) and one in-fragment π NFBO of the outer layer (Fig. 7d). Due to space limitations, only four selected bonding interactions are shown in detail with both NFBOs and NFHOs in Fig. 8. For all the non-trivial NFBOs and NFHOs of B_{19}^-, see Fig. S1 through Fig. S7. In total, we find two π

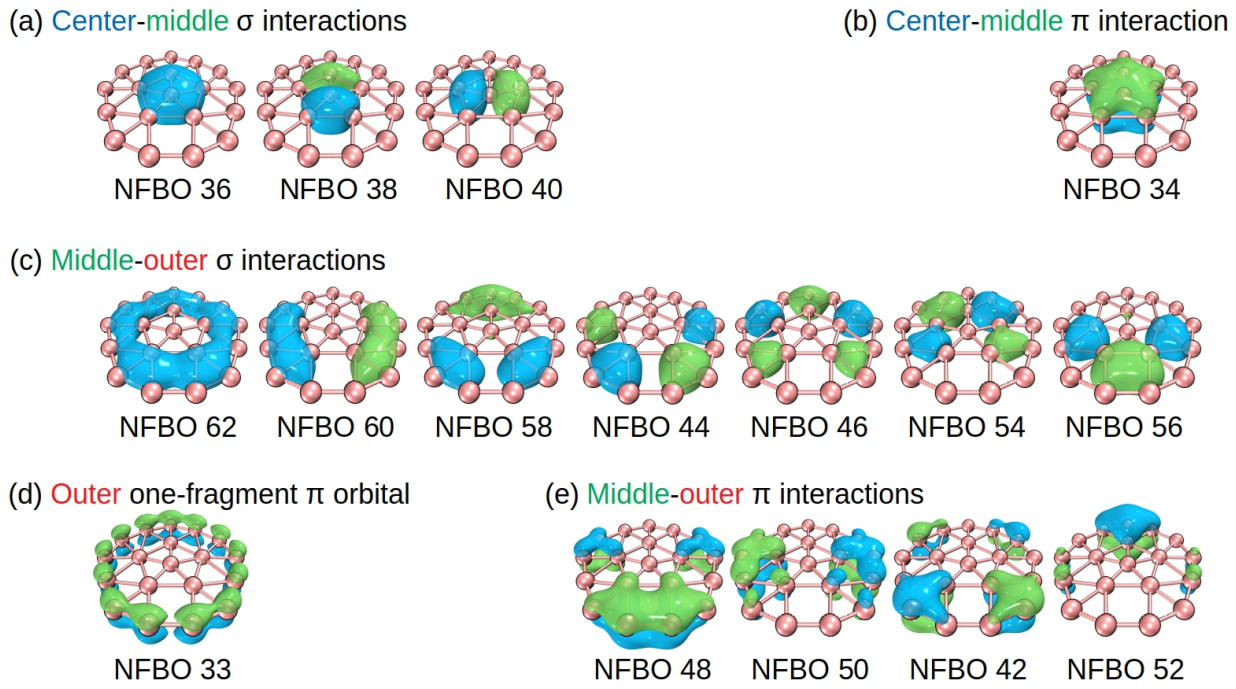

Figure 7: Non-anti-bonding NFBOs of B_{19}^- with C_{2v} symmetry: (a) The bonding σ NFBOs of center-middle interaction; (b) The bonding π NFBOs of center-middle interaction; (c) The bonding σ NFBOs of middle-outer interaction; (d) The non-bonding π NFBO of the outer layer; (e) The bonding π NFBOs of middle-outer interaction. The $1s$ core orbitals and the thirteen B−B single bond orbitals of the outer layer are trivial and not shown.

and six σ electrons between the center and the middle layer, as well as ten π and fourteen σ electrons between the middle layer and the outer layer. In this way, we obtain the same scheme of inner $2\pi/6\sigma$ and outer $10\pi/14\sigma$ aromaticity of B_{19}^- as put forward in Ref. 47. Clearly, the electron configurations of 2π, 6σ, 10π and 14σ, each satisfying Huckel's $4n+2$ rule, provide an explanation for the remarkable stability observed in the cluster. Finally, note that no artificial parameters except the fragmentation and the threshold are invoked,

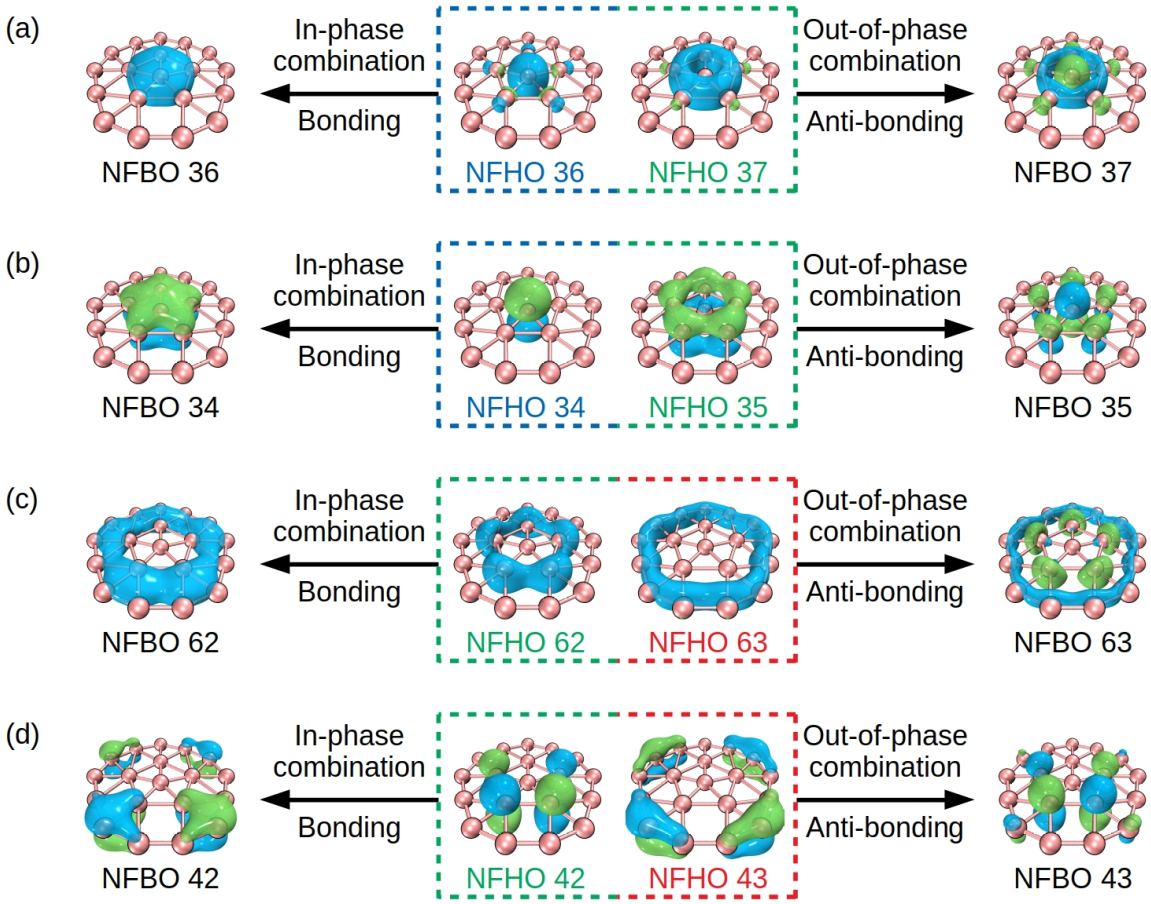

Figure 8: Detailed bonding interactions for selected NFBOs shown in Fig. 7. The colors of the texts and dashed boxes suggest the fragments (shown in Fig. 6b) from which the NFHOs originate.

making NFBO analysis a convenient tool less subject to human interference.

4.4 $[Sn_7I_7P_7]_n$: a double helical structure

In the final example, we will illustrate how the fragment-based view extends to periodic systems.

The first atomic-scale double helical semiconductor, $[Sn_7I_7P_7]_n$, was reported in 2016.[29] In $[Sn_7I_7P_7]_n$, two chains, $[Sn_7I_7]_n$ and $[P_7]_n$, are winded together analogous to the two chains in DNA. Electron localization function (ELF) analysis[48] shows dative bonds donated from the inner phosphorus atoms to the outer tin atoms, accounting for the inter-chain binding force.[29,49] However, ELF analysis does not give sufficient information on the components of these bonds, which is crucial for understanding the origin of the double helical structure. We have found that our NFBO analysis can fill the gap and explain why the double helical structure is stable for $[Sn_7I_7P_7]_n$.

The DFT computation is done with the density functional BLYP,[50,51] the basis set def2-SVP[52] and the density fitting basis set W06[53] to one unit cell of $[Sn_7I_7P_7]_n$. Ten k points are used for optimization, while the Γ point alone is used for NFBO analysis. The optimized bond angles with regard to a tin atom and its neighboring atoms are $\angle$I$-$Sn$-$I $= 158.3°$, $\angle$P$-$Sn$-$I $= 78.2°,\ 85.9°$ and $\angle$P$-$Sn$-$P $= 85.7°$.

To find the interaction between a Sn atom with its surroundings, we set one of the Sn atoms as one fragment, the rest of the $[Sn_7I_7]$ chain as the second fragment and the P atoms as the last two fragments (Fig. 9a). The $[P_7]$ chain is divided into two fragments in a way that the two P atoms having dative interactions with the first Sn atom come from different fragments (Fig. 9a).

Figures 9b-e list all the bonding schemes involving the valence electrons of the first Sn atom: NFBO or NFHO 10 is the non-bonding valence s orbital of Sn; NFBOs 202 and 203 feature the 3c-2e bonds between the Sn and its neighboring I atoms, involving the p orbitals of the three atoms indicated by NFHOs 202 and 203; NFBOs 204 through 207 illustrate the

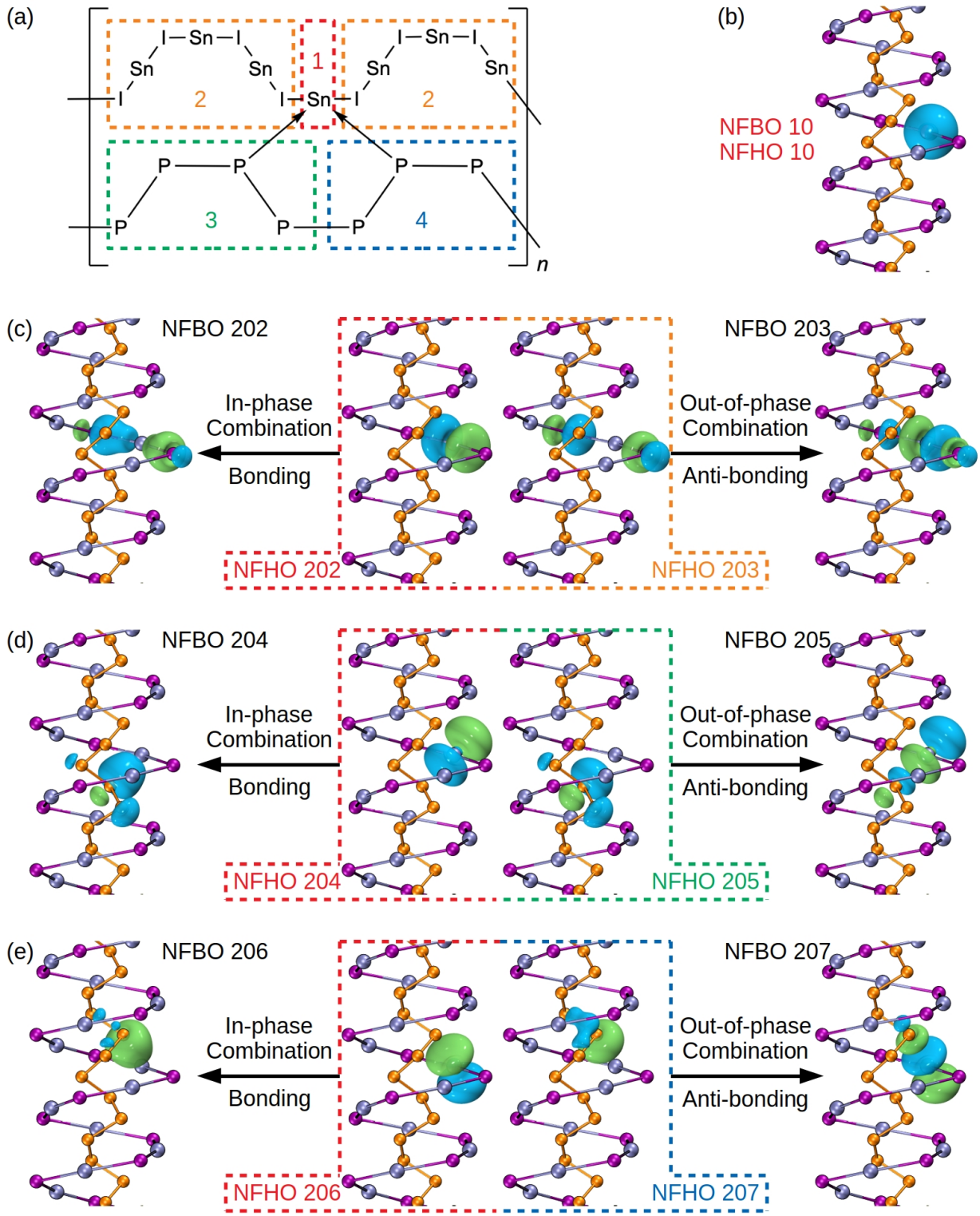

Figure 9: (a) The fragmentation and (b-e) bonding schemes of $[Sn_7I_7P_7]_n$. (b) The non-bonding s orbital of Sn; (c) The delocalized [I−Sn−I] σ bond consisting of one p orbital of Sn and I; (d,e) The localized [P−Sn] bonds consisting of the other two p orbitals of Sn and the sp^3 orbitals of P. The colors of the texts and dashed boxes in (b-e) suggest the fragments in (a) from which the NFHOs originate.

localized dative bonds to the Sn atom from its neighboring P atoms, concerning the other two valence p orbitals of the Sn atom and the sp^3 orbitals of the P atom.

It is noteworthy that the Sn atom is barely hybridized: its valence s orbital is inactive and its three valence p orbitals bond with the ligands individually. The bonding situation is similar to those in PF_3 and SbF_3 where each P−F or Sb−F bond involves one of the p orbitals of the center atom alone without any significant s character. The inert valence Sn s orbital accommodates the inert pair of valence s electrons, rendering the metal center formally Sn(II). The utilization of the three Sn valence p orbitals for bonding with I and P results in the observations of the bond angles, ∠P−Sn−P and ∠P−Sn−I, which are all nearly 90°. The double helical structure of $[Sn_7I_7P_7]_n$ facilitates the optimal Sn−I and Sn−P bonding interactions.

This example demonstrates the application of NFBO to examining bonding interactions in periodic solid state systems. Although an atom-centered gaussian basis set is utilized here, plane-wave-based wavefunctions can also benefit from the NFBO method via plane-wave-to-atomic-orbital projection.[30]

5 Summary

In this paper, we present the natural fragment bond orbital (NFBO) method for inter-fragment bonding interaction analysis, as an extension to the well-known natural bond orbital method. This newly developed NFBO method was applied to analyze bonding interactions in various systems, including the transition state of a Diels-Alder reaction, tri-nuclear clusters of zinc and thorium, the B_{19}^- cluster and the double helical $[Sn_7I_7P_7]_n$ structure. These analyses demonstrate the effectiveness and power of the NFBO method for investigating bonding interactions in complex molecular systems.

Code availability

The program we have developed for NFBO analysis, `Orbaplaw`, can be freely obtained from its homepage https://github.com/FreemanTheMaverick/Orbaplaw, where the user guidance and several extra examples can also be found. These examples include a tri-titanium polyhydride complex,[46] a uranium-cyclobutadiene-uranium sandwich structure[54] and the transition state of an organo-palladium catalyzed aryldifluoromethylation reaction.[55]

Supplementary material

The supplementary material is available at https://doi.org/10.26434/chemrxiv-2024-rt585. It contains all the non-trivial NFBOs and NFHOs of B_{19}^-.

Acknowledgement

We thank Prof. Frank Weinhold for explaining algorithmic details on NAO construction, Dr. Lu Tian for providing technical support in using `Multiwfn` and Mr. Chan Ka Lok for constructive comments on the manuscript. We also thank the Research Grants Council of Hong Kong (HKUST 16302222) for financial support.

References

(1) Edmiston, C.; Ruedenberg, K. Localized atomic and molecular orbitals. *Rev. Mod. Phys.* **1963**, *35*, 457–464.

(2) Foster, J. M.; Boys, S. F. Canonical configurational interaction procedure. *Rev. Mod. Phys.* **1960**, *32*, 300–302.

(3) Pipek, J.; Mezey, P. G. A fast intrinsic localization procedure applicable for *ab initio*

and semiempirical linear combination of atomic orbital wave functions. *J. Chem. Phys.* **1989**, *90*, 4916–4926.

(4) Lehtola, S.; Jónsson, H. Unitary optimization of localized molecular orbitals. *J. Chem. Theory Comput.* **2013**, *9*, 5365–5372.

(5) Zhang, J.-X.; Sheong, F. K.; Lin, Z. Unravelling chemical interactions with principal interacting orbital analysis. *Chem. Eur. J.* **2018**, *24*, 9639–9650.

(6) Sheong, F. K.; Zhang, J.-X.; Lin, Z. Principal interacting spin orbital: Understanding the fragment interactions in open-shell systems. *Phys. Chem. Chem. Phys.* **2020**, *22*, 10076–10086.

(7) Zhang, J.-X.; Sheong, F. K.; Lin, Z. Principal interacting orbital: A chemically intuitive method for deciphering bonding interaction. *WIREs Comput. Mol. Sci.* **2020**, *10*, e1469.

(8) Sheong, F. K.; Chen, W.-J.; Zhang, J.-X.; Li, Y.; Lin, Z. Structure and bonding of $[Pd_2Sn_{18}]^{4-}$: An interesting example of the mutual delocalisation phenomenon. *Dalton Trans.* **2017**, *46*, 2214–2219.

(9) Zhang, J.-X.; Sheong, F. K.; Lin, Z. Remote bonding in clusters $[Pd_3Ge_{18}R_6]^{2-}$: Modular bonding model for large clusters via principal interacting orbital analysis. *Inorg. Chem.* **2019**, *58*, 3473–3478.

(10) Sheong, F. K.; Zhang, J.-X.; Lin, Z. Modular bonding picture for aromatic borometallic molecular wheels. *Theor. Chem. Acc.* **2020**, *139*, 14.

(11) Foster, J. P.; Weinhold, F. Natural hybrid orbitals. *J. Am. Chem. Soc.* **1980**, *102*, 7211–7218.

(12) Reed, A. E.; Curtiss, L. A.; Weinhold, F. Intermolecular interactions from a natural bond orbital, donor-acceptor viewpoint. *Chem. Rev.* **1988**, *88*, 899–926.

(13) Badenhoop, J. K.; Weinhold, F. Natural bond orbital analysis of steric interactions. *J. Chem. Phys.* **1997**, *107*, 5406–5421.

(14) Glendening, E. D.; Landis, C. R.; Weinhold, F. Natural bond orbital methods. *WIREs Comput. Mol. Sci.* **2012**, *2*, 1–42.

(15) Weinhold, F. Natural bond orbital analysis: A critical overview of relationships to alternative bonding perspectives. *J. Comput. Chem.* **2012**, *33*, 2363–2379.

(16) Leyssens, T.; Peeters, D.; Orpen, A. G.; Harvey, J. N. How important is metal-ligand back-bonding toward YX3 ligands (Y = N, P, C, Si)? An NBO analysis. *Organometallics* **2007**, *26*, 2637–2645.

(17) Algarra, A. G.; Grushin, V. V.; Macgregor, S. A. Natural bond orbital analysis of the electronic structure of [LnM(CH_3)] and [LnM(CF_3)] complexes. *Organometallics* **2012**, *31*, 1467–1476.

(18) Nova, A.; Suh, H.-W.; Schmeier, T. J.; Guard, L. M.; Eisenstein, O.; Hazari, N.; Maseras, F. An unusual example of hypervalent silicon: A five-coordinate silyl group bridging two palladium or nickel centers through a nonsymmetrical four-center two-electron bond. *Angew. Chem. Int. Ed.* **2014**, *53*, 1103–1108.

(19) Landis, C. R.; Weinhold, F. 18-electron rule and the 3c/4e hyperbonding saturation limit. *J. Comput. Chem.* **2016**, *37*, 237–241.

(20) Gomes, G. d. P.; Vil, V.; Terentev, A.; Alabugin, I. V. Stereoelectronic source of the anomalous stability of bis-peroxides. *Chem. Sci.* **2015**, *6*, 6783–6791.

(21) Reed, A. E.; Weinhold, F. Natural localized molecular orbitals. *J. Chem. Phys.* **1985**, *83*, 1736–1740.

(22) Glendening, E. D.; Weinhold, F. Natural resonance theory: I. General formalism. *J. Comput. Chem.* **1998**, *19*, 593–609.

(23) Glendening, E. D.; Landis, C. R.; Weinhold, F. Resonance theory reboot. *J. Am. Chem. Soc.* **2019**, *141*, 4156–4166.

(24) Zubarev, D. Y.; Boldyrev, A. I. Developing paradigms of chemical bonding: Adaptive natural density partitioning. *Phys. Chem. Chem. Phys.* **2008**, *10*, 5207–5217.

(25) Glendening, E. D.; Weinhold, F. Resonance natural bond orbitals: Efficient semilocalized orbitals for computing and visualizing reactive chemical processes. *J. Chem. Theory Comput.* **2019**, *15*, 916–921.

(26) Freitag, K.; Gemel, C.; Jerabek, P.; Oppel, I. M.; Seidel, R. W.; Frenking, G.; Banh, H.; Dilchert, K.; Fischer, R. A. The σ-aromatic clusters $[Zn_3]^+$ and $[Zn_2Cu]$: Embryonic brass. *Angew. Chem. Int. Ed.* **2015**, *54*, 4370–4374.

(27) Boronski, J. T.; Seed, J. A.; Hunger, D.; Woodward, A. W.; van Slageren, J.; Wooles, A. J.; Natrajan, L. S.; Kaltsoyannis, N.; Liddle, S. T. A crystalline tri-thorium cluster with σ-aromatic metal–metal bonding. *Nature* **2021**, *598*, 72–75.

(28) Huang, W.; Sergeeva, A. P.; Zhai, H.-J.; Averkiev, B. B.; Wang, L.-S.; Boldyrev, A. I. A concentric planar doubly π-aromatic B_{19}^- cluster. *Nat. Chem.* **2010**, *2*, 202–206.

(29) Pfister, D. et al. Inorganic double helices in semiconducting SnIP. *Adv. Mater.* **2016**, *28*, 9783–9791.

(30) Dunnington, B. D.; Schmidt, J. R. Generalization of natural bond orbital analysis to periodic systems: Applications to solids and surfaces via plane-wave density functional theory. *J. Chem. Theory Comput.* **2012**, *8*, 1902–1911.

(31) Becke, A. D. Density-functional thermochemistry. III. The role of exact exchange. *J. Chem. Phys.* **1993**, *98*, 5648–5652.

(32) Hariharan, P. C.; Pople, J. A. The influence of polarization functions on molecular orbital hydrogenation energies. *Theor. Chim. Acta* **1973**, *28*, 213–222.

(33) Frisch, M. J. et al. Gaussian 16 Revision C.01. 2016; Gaussian Inc. Wallingford CT.

(34) Reed, A. E.; Weinstock, R. B.; Weinhold, F. Natural population analysis. *J. Chem. Phys.* **1985**, *83*, 735–746.

(35) Lu, T.; Chen, F. Multiwfn: A multifunctional wavefunction analyzer. *J. Comput. Chem.* **2012**, *33*, 580–592.

(36) Zhang, Y. Orbaplaw: Orbital alignment analysis for plane wave basis sets. https://github.com/FreemanTheMaverick/Orbaplaw, 2024.

(37) Humphrey, W.; Dalke, A.; Schulten, K. VMD: Visual molecular dynamics. *J. Mol. Graphics* **1996**, *14*, 33–38.

(38) Hehre, W. J.; Stewart, R. F.; Pople, J. A. Self-Consistent Molecular-Orbital Methods. I. Use of Gaussian Expansions of Slater-Type Atomic Orbitals. *J. Chem. Phys.* **1969**, *51*, 2657–2664.

(39) Carlson, B. C.; Keller, J. M. Orthogonalization procedures and the localization of wannier functions. *Phys. Rev.* **1957**, *105*, 102–103.

(40) Yu, J.; Su, N. Q.; Yang, W. Describing chemical reactivity with frontier molecular orbitalets. *JACS Au* **2022**, *2*, 1383–1394.

(41) Sheong, F. K.; Zhang, J.-X.; Lin, Z. Localized bonding model for coordination and cluster compounds. *Coord. Chem. Rev.* **2017**, *345*, 42–53.

(42) Cuyacot, B. J. R.; Foroutan-Nejad, C. $[\{Th(C_8H_8)Cl_2\}_3]^{2-}$ is stable but not aromatic. *Nature* **2022**, *603*, E18–E20.

(43) Boronski, J. T.; Seed, J. A.; Hunger, D.; Woodward, A. W.; van Slageren, J.; Wooles, A. J.; Natrajan, L. S.; Kaltsoyannis, N.; Liddle, S. T. Reply to: $[\{Th(C_8H_8)Cl_2\}_3]^{2-}$ is stable but not aromatic. *Nature* **2022**, *603*, E21–E22.

(44) Küchle, W.; Dolg, M.; Stoll, H.; Preuss, H. Energy-adjusted pseudopotentials for the actinides. Parameter sets and test calculations for thorium and thorium monoxide. *J. Chem. Phys.* **1994**, *100*, 7535–7542.

(45) Demadis, K. D.; Hartshorn, C. M.; Meyer, T. J. The localized-to-delocalized transition in mixed-valence chemistry. *Chem. Rev.* **2001**, *101*, 2655–2686.

(46) Shima, T.; Hu, S.; Luo, G.; Kang, X.; Luo, Y.; Hou, Z. Dinitrogen cleavage and hydrogenation by a trinuclear titanium polyhydride complex. *Science* **2013**, *340*, 1549–1552.

(47) Li, R.; You, X.-R.; Guo, J.-C.; Zhai, H.-J. Concentric inner $2\pi/6\sigma$ and outer $10\pi/14\sigma$ aromaticity underlies the dynamic structural fluxionality of planar B_{19}^- Wankel motor cluster. *J. Phys. Chem. A* **2021**, *125*, 5022–5030.

(48) Becke, A. D.; Edgecombe, K. E. A simple measure of electron localization in atomic and molecular systems. *Theor. Chim. Acta* **1990**, *92*, 5397–5403.

(49) Li, X.; Dai, Y.; Ma, Y.; Li, M.; Yu, L.; Huang, B. Landscape of DNA-like inorganic metal free double helical semiconductors and potential applications in photocatalytic water splitting. *J. Mater. Chem. A* **2017**, *5*, 8484–8492.

(50) Becke, A. D. Density-functional exchange-energy approximation with correct asymptotic behavior. *Phys. Rev. A* **1988**, *38*, 3098–3100.

(51) Lee, C.; Yang, W.; Parr, R. G. Development of the Colle-Salvetti correlation-energy formula into a functional of the electron density. *Phys. Rev. B* **1988**, *37*, 785–789.

(52) Weigend, F.; Ahlrichs, R. Balanced basis sets of split valence, triple zeta valence and quadruple zeta valence quality for H to Rn: Design and assessment of accuracy. *Phys. Chem. Chem. Phys.* **2005**, *7*, 3297–3305.

(53) Weigend, F. Accurate Coulomb-fitting basis sets for H to Rn. *Phys. Chem. Chem. Phys.* **2006**, *8*, 1057–1065.

(54) Patel, D.; McMaster, J.; Lewis, W.; Blake, A. J.; Liddle, S. T. Reductive assembly of cyclobutadienyl and diphosphacyclobutadienyl rings at uranium. *Nat. Commun.* **2013**, *4*, 2323.

(55) Choi, K.; Mormino, M. G.; Kalkman, E. D.; Park, J.; Hartwig, J. F. Palladium-catalyzed aryldifluoromethylation of aryl halides with aryldifluoromethyl trimethylsilanes. *Angew. Chem. Int. Ed.* **2022**, *61*, e202208204.